PHYSICAL REVIEW B **79**, 245331 (2009)

Topological insulators in three dimensions from spontaneous symmetry breaking

Yi Zhang,[1] Ying Ran,[1,2] and Ashvin Vishwanath[1,2]
[1]Department of Physics, University of California, Berkeley, California 94720, USA
[2]Materials Sciences Division, Lawrence Berkeley National Laboratory, Berkeley, California 94720, USA

(Received 20 April 2009; revised manuscript received 12 June 2009; published 30 June 2009)

We study three-dimensional systems where strong repulsion leads to an insulating state via spontaneously generated spin-orbit interactions. We discuss a microscopic model where the resulting state is topological. Such topological "Mott" insulators differ from their band-insulator counterparts in that they possess an additional order parameter, a rotation matrix, which describes the spontaneous breaking of spin-rotation symmetry. We show that line defects of this order are associated with protected one-dimensional modes in the *strong* topological Mott insulator that provides a bulk characterization of this phase. Possible physical realizations in cold-atom systems are discussed.

DOI: 10.1103/PhysRevB.79.245331 PACS number(s): 73.43.−f, 71.30.+h, 71.10.Fd

I. INTRODUCTION

Seminal work by Thouless and co-workers[1] pointed out that band insulators are not identical but can differ in fundamental respects that are characterized by a topological property of the bands. The central example discussed was the integer quantum-Hall state, whose topological properties are characterized by an integer that is essentially the Hall conductance. Realizing such a state naturally requires breaking of time-reversal symmetry typically by the application of a strong magnetic field on a two-dimensional (2D) system. The topological nature of the integer quantum-Hall state is also revealed by studying the edge of a two-dimensional sample, where chiral (one way propagating) edge states occur at energies within the bulk energy gap.

Recently, it has been realized that band insulators with spin-orbit interactions can also be characterized by their band topology. In two dimensions, the quantum spin-Hall (QSH) phase is closely analogous to the quantum-Hall state. However, since it preserves time-reversal symmetry, it has a pair of counterpropagating one-dimensional modes at the edge. Such a state can occur with spin-orbit interactions that preserve spin-rotation symmetry (SRS) about an axis.[2,3] It was shown in Ref. 3 that even in the absence of such spin-rotation invariance, the counterpropagating modes remain protected by time-reversal symmetry. The topological properties of these insulators are characterized not by an integer but by a Z_2 number (0,1) so that all topologically nontrivial insulators of this kind fall within the same topological class. An experimental realization of this phase has been reported in HgTe heterostructures.[4,5]

Turing to three dimensions, an insulator with nontrivial band topology can be realized just by stacking such 2D QSH states. These are called the weak topological insulators weak TIs. However, a more surprising possibility, the strong TI, has been predicted theoretically.[6–8] Once again, the surface physics is exotic, which provides a physical characterization of this phase. Strong TI have an odd number of Dirac nodes on their surface, which are stable against moderate perturbations that preserve time-reversal symmetry.[6] Such a band structure cannot be realized in any two-dimensional system with time-reversal invariance. There have been experimental realizations of these predictions in bismuth antimony[9–11] alloys and in bismuth selenium,[12,13] which have been verified by angle-resolved photoemission spectroscopy. Note, in contrast to the quantum spin-Hall state, that in order to realize the TI the SRS must be completely broken.

The TI and QSH phases normally exist in systems with strong spin-orbit interaction that explicitly breaks SRS.[3,6,14] However, as pointed out in Ref. 15 an extended Hubbard model on a 2D honeycomb lattice can have spontaneous SRS breaking and result in a QSH phase, with the right kind of repulsive interactions.[15] SRS is only preserved about an axis $\hat{n}$, which is spontaneously chosen, leading to gapless Goldstone modes. This was termed as a topological "Mott" insulator—the separation of energy scales between the low-lying magnetic excitations and the gapped charge excitations being typical of Mott insulators. We will also adopt this nomenclature although it must be noted that local-moment physics, often associated with Mott insulators, does not occur here. Subsequently, it was argued in Ref. 16 that skyrmions of $\hat{n}$ carry charge $2e$.

Here, we consider the analogous problem of a three-dimensional (3D) system without bare spin-orbit couplings and full SRS, being driven into a TI state by strong interactions. The key difference from the two-dimensional case is that in order to realize the strong TI, SRS must be completely broken. Hence the order parameter in this case is a rotation matrix $\overleftrightarrow{\boldsymbol{R}} \in \mathrm{O}(3)$, similar to superfluid helium-3 A and B phases. Physically, this order parameter describes the orientation of the spin-coordinate system, relative to the spatial coordinates. Spatial variations in the order parameter lead to a rich set of topological textures. We describe a microscopic model, an extended Hubbard model on the diamond lattice that, within a mean-field treatment, leads to this phase. The order parameter supports a number of topological defects. In particular, a vortexlike line defect occurs but with a Z_2 charge. This line defect in the *strong* TI is found to be associated with a pair of gapless fermionic excitations that travel along its length. These modes are topologically stable against moderate perturbations such as impurities and interactions as long as time-reversal symmetry is intact. This is the main result of the paper—an analytical derivation is provided, which relies on the properties of the Dirac equation on a two-dimensional curved surface.

We now contrast our results with other recent work. Similar exotic behavior also occurs in TIs along with crystal defects such as dislocations. Gapless fermionic excitations emerge there when a Z_2 parameter formed by the product of the dislocation Burgers vector and three weak TI indices[17] is nonzero, which, in principle, can occur in both the weak and strong TIs. In contrast, in the present paper, the fermionic modes along the line defect are solely determined by the more elusive strong index. They are absent in the case of the weak TI. Thus far, the characterization of the TI phase has relied on the surface behavior. This result provides a route to identifying the strong topological Mott insulator via a bulk property.

Similar modes have been identified propagating along a solenoid of π flux, inserted into a strong TI.[18] Here, the 2π rotation of the electron spin around the line defect leads to a Berry's phase, providing a physical realization of the π flux. Analogous phenomena occur in the context of line defects in superfluid He_3-B.[19]

The order parameter $\overleftrightarrow{\boldsymbol{R}}$ also admits a skyrmionlike texture, which is a point object in three dimensions (Shankar monopole). We find that in contrast to the skyrmion of the quantum spin-Hall effect,[16] these are uncharged.

Most solids where electron-electron interactions are important tend to have some degree of spin-orbit interactions, which will confine the defects. Hence, we propose realizations of this physics in optical lattices of ultracold atoms, utilizing molecules with multipole moments to obtain the proposed extended Hubbard models. The two-dimensional version[15] is found to be naturally realized with electric dipoles. Realizing the three-dimensional case is more challenging; however molecules with electric quadrupole moments confined in optical lattice can realize some of the key ingredients required.

This paper is organized as the following: In Sec. II, we will present the order-parameter manifold and the line modes' Z_2 dependence on the winding number; in Sec. III, we will justify our claim with numerical and analytical results; another texture Shankar monopole will be discussed in Sec. IV; in Sec. V, we will establish our model Hamiltonian on a diamond lattice and show the mean-field stability of topological Mott insulating (TMI) phases; we give two possible experimental realizations in cold-atom systems in Sec. VI; and we conclude the main result of this paper in Sec. VII. Hereafter we use σ and τ for the spin and sublattice degree of freedom, respectively.

II. TOPOLOGICAL MOTT INSULATORS AND ORDER-PARAMETER TEXTURES IN THREE DIMENSIONS

In order to describe the TMI phase, we consider a concrete example in the following. In Sec. V, we address the question of how such a phase may be microscopically realized. To contrast the TMI phase with the regular topological insulator, consider the model Hamiltonians of a TI introduced in Ref. 6. We consider nearest-neighbor hopping (t_{ij}) on the sites of a diamond lattice and spin-orbit-induced hopping on next-neighbor sites,

$$H_{\mathrm{TI}} = H_{\mathrm{hop}} + H_{\mathrm{SO}},$$

$$H_{\mathrm{hop}} = \sum_{\langle ij\rangle} t_{ij} c_i^{\dagger} c_j,$$

$$H_{\mathrm{SO}} = i(8\lambda_{\mathrm{SO}}/a^2) \sum_{\langle\langle ij\rangle\rangle} c_i^{\dagger} \vec{\sigma} \cdot (\vec{d}_{ij}^{\,1} \times \vec{d}_{ij}^{\,2}) c_j, \qquad (1)$$

where $c^{\dagger} = (c_{\uparrow}^{\dagger}, c_{\downarrow}^{\dagger})$ is the electron-creation operator and $\vec{\sigma}$ is the spin Pauli matrix. The spin-orbit interaction for a pair of second-neighbor sites ij depends on d_{ij}^{p} $(p=1,2)$, the two nearest-neighbor bond vectors connecting the second-neighbor sites ij. The spin-orbit interactions are thus determined by the crystal structure. Note that the SU(2) SRS is completely broken, which is required to realize the strong TI in three dimensions.

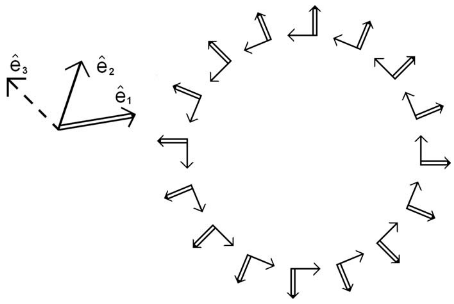

FIG. 1. An illustration of order parameter $\boldsymbol{R}$ of a nontrivial line defect in the x-y plane and $\hat{z}$ direction is translation invariant. The hollow and solid arrows are the $\hat{x}$ and $\hat{y}$ axes of local coordinate; the $\hat{z}$ axis points out of the paper for proper rotation.

In contrast, in the TMI phase discussed here, the underlying Hamiltonian possesses full SU(2) SRS that is *spontaneously* broken. The order parameter $\overleftrightarrow{\boldsymbol{R}}$ then is a rotation matrix that describes the relative orientation between the real-space coordinate system and the spin axes. The spin-orbit term then takes the form

$$H_{\mathrm{SO}}^{\mathrm{TMI}} = i(8\lambda_{\mathrm{SO}}/a^2) \sum_{\langle\langle ij\rangle\rangle} c_i^{\dagger} \vec{\sigma} \cdot \overleftrightarrow{\boldsymbol{R}}_{\boldsymbol{l}} \cdot (\vec{d}_{ij}^{\,1} \times \vec{d}_{ij}^{\,2}) c_j. \qquad (2)$$

There is one important difference between the TI and TMI: since in the latter $\overleftrightarrow{\boldsymbol{R}}$ arises from symmetry breaking it can vary spatially to give rise to a topologically nontrivial texture. To identify the topologically stable defects, we first note that the order-parameter manifold is a three-dimensional orthogonal matrix $\overleftrightarrow{\boldsymbol{R}} \in \mathrm{O}(3)$. It can be represented by $\overleftrightarrow{\boldsymbol{R}} = (\hat{e}_1, \hat{e}_2, \hat{e}_3)$, where $\hat{e}_i$ are orthogonal unit vectors representing the basis vectors of the spin-coordinate system. An example is shown in Fig. 1.

The target manifold of this order parameter is $O(3) = \mathrm{SO}(3) \times Z_2$ and Z_2 determines the chirality $\det(\overleftrightarrow{\boldsymbol{R}}) = \pm 1$ or whether the rotation is proper or improper. Hereafter we mainly focus on the continuous SO(3) part of the order parameter for it has nontrivial homotopy groups in two and three dimensions. Then, each proper rotation can be described by the parameters $(\hat{n}, \theta)$, where $\hat{n}$ is the direction of the rotation axis and $\theta \in [0, \pi]$ is the rotation angle around it. To visualize it we can map all proper rotation matrices to a solid ball with radius π, where $\hat{n}$ maps to the radial direction and rotation angle maps to the radius of the image point. Note that a rotation of π about $\hat{n}$ is the same as that of π about $-\hat{n}$, so opposite points on the spherical surface are identified. The resulting geometry is a three-dimensional projective plane P^3.[20]

We now discuss the topological defects of this order-parameter space. The discrete Z_2 symmetry breaking implied by the $Z_2 \times \mathrm{SO}(3)$ order parameter leads to domain walls in three dimensions. More interestingly, line defects also exist (we assume three spatial dimensions in the following). These can be captured by considering the order parameter along a closed curve in real space, which encircles the line defect. This defines a closed loop in the order-parameter space and distinct classes of such closed loops correspond to the topological line defects. There are two classes of closed loops for the SO(3) space described above. In addition to the trivial closed loop, which can be shrunk continuously to a point, there exists a nontrivial loop that connects the antipodal points $(\hat{n},\pi)$ and $(-\hat{n},\pi)$. Since these represent the same rotation, this is, in fact, a closed loop. Thus there is a nontrivial line defect characterized just by a Z_2 topological charge. Technically $\pi_1[\mathrm{SO}(3)]=Z_2$.[20] An example is shown in Fig. 1 with translational invariance along z direction although generically the line can be of arbitrary shape and direction. The electronic properties of such a line defect are studied in Sec. III—protected one-dimensional modes that propagate along the defect are found in the case of the strong TMI but not in the case of the weak TMI. We also note that since $\pi_2[\mathrm{SO}(3)]=0$, no nontrivial point defects exist in three dimensions. However, since $\pi_3[\mathrm{SO}(3)]=Z$, "skyrmionlike" textures (called Shankar monopoles[21]) exist in three dimensions. In contrast to topological defects, they are smooth textures without a singular core. We investigate the electronic structure of these objects and find that they are neutral in the large size limit, in contrast to skyrmions in the two-dimensional quantum spin-Hall state, which carry charge $2e$.[16]

III. ELECTRONIC STRUCTURE OF A LINE DEFECT: NUMERICAL AND ANALYTICAL RESULTS

We study the electronic structure of the Z_2 line defect in the diamond-lattice model of a TMI discussed before. We choose the nearest-neighbor hopping in three directions to be equal, $t_{ij}=t>0$, while the fourth is different, $t_{ij}=t+\delta t$. A strong (weak) TI phase occurs if $\delta t>0$ ($\delta t<0$).[6] We choose an order-parameter texture that incorporates line defects,

$$H=\sum_{\langle ij\rangle} t_{ij} c_i^\dagger c_j + i(8\lambda_{\mathrm{SO}}/a^2)\sum_{\langle\langle ij\rangle\rangle} c_i^\dagger \vec{s}\cdot \overleftrightarrow{\boldsymbol{R}}_l \cdot (\vec{d}_{ij}^{1}\times \vec{d}_{ij}^{2})c_j, \quad (3)$$

with

$$\overleftrightarrow{\boldsymbol{R}}_l(\varphi)=\begin{pmatrix} \cos(l\varphi) & \sin(l\varphi) & 0 \\ -\sin(l\varphi) & \cos(l\varphi) & 0 \\ 0 & 0 & 1 \end{pmatrix},$$

where $\overleftrightarrow{\boldsymbol{R}}_l$ depends only on the azimuthal angle of the atom connecting sites i and j. Note that only the parity of l is topologically stable. Here we study a system of 24×24 with a maximally separated vortex ($l=1$) and antivortex ($l=-1$) and with periodic boundary condition in x-y plane and translational invariance in z direction. Note that time-reversal symmetry is preserved by this Hamiltonian.

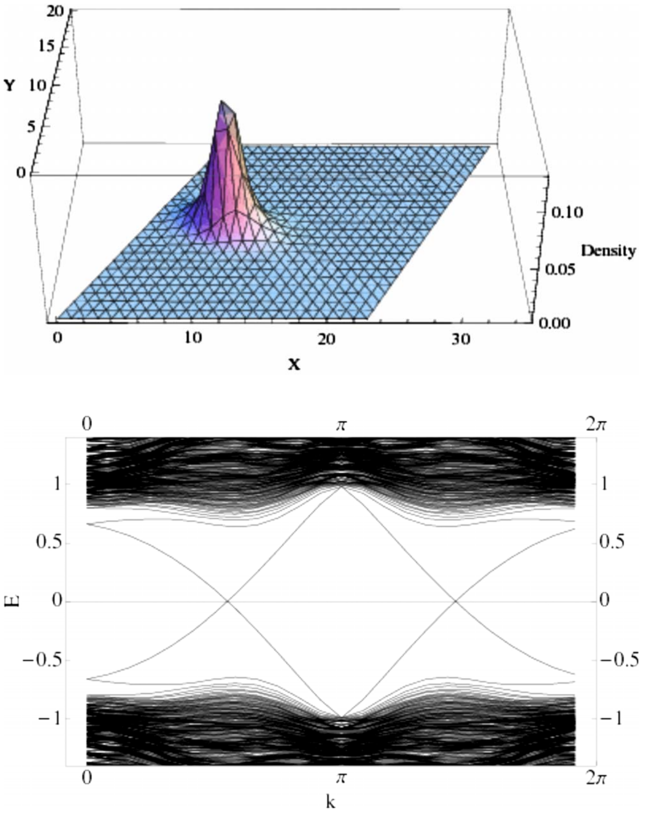

FIG. 2. (Color online) Up: the density distribution of a midgap mode ($k=1.05, E=0.25$) in the $\vec{a}_1,\vec{a}_2$ plane, the mode is well localized at the $l=1$ vortex and the other state ($k=1.05, E=-0.25$) is well localized at the $l=-1$ antivortex. Down: electronic spectrum of diamond lattice strong TMI along p_z in the presence of a pair of defects. The parameters used in the Hamiltonian are $t=1.0$, $\delta t=1.0$, and $\lambda_{\mathrm{SO}}=0.125$.

For a $\delta t>0$ strong TMI system with $l=\pm 1$, two pairs of conducting line modes are found in the bulk gap. These states' density profiles are strongly localized at the cores or the two defects [Fig. 2 (top) shows only one of them for clarity]. Therefore a Kramer pair of modes is localized along the thread of core. Given the particle-hole symmetry that happens to be present in this model, they cross at zero energy [Fig. 2 (bottom)]. In contrast, these modes are *absent* in the cases of the weak TMI $\delta t<0$ or if $l=0,\pm 2$ in either type of TMI and the band structure remains fully gapped. This is direct evidence that these Z_2-dependent line modes within the bulk identify the strong TMI.

An analytical argument for these modes can be developed in several ways. We can derive these modes based on the 3D Dirac continuum limit of Hamiltonian (3); however, below we consider deriving these modes using the known properties of surface states of strong TI. Consider a bulk sample with a infinitely long cylindrical hole of radius R drilled through its center. We consider the low-energy states on the cylindrical surface, both without and with a line defect inserted in the cylindrical hole (Fig. 3). We show that in the

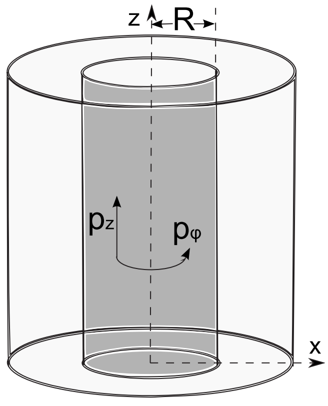

FIG. 3. Illustration for the model on an effective Hamiltonian on a curved surface we study. The radius of the cylinder is R with strong TMI outside and vacuum inside. p_z and p_φ are momentum along $\hat{z}$ and the azimuthal direction, respectively. θ is the angle between $\vec{\sigma}'$ and $\vec{p}$.

limit of $R \to 0$, a propagating midgap mode survives only when the defect is present, otherwise a fully gapped insulator results. Interestingly, the key ingredient here is the property of the two-dimensional surface-Dirac state on a curved manifold. In contrast to the states of a particle on a ring, where the zero angular momentum eigenstate remains at low energy even when the ring radius is shrunk to zero, here, the Dirac particle acquires a Berry's phase of π on rotating around the cylinder surface, which excludes the zero angular momentum state. Hence on shrinking the radius, no low-energy states remain and the bulk insulator is recovered. However, if a topological defect of the spin-orbit coupling matrix is inserted through the cylinder, an additional Berry's phase of π is now acquired by the electrons. This ultimately results from the rotation of the electron's spin by 2π on following the texture. With this additional phase, the zero angular momentum mode is allowed and a low-energy propagating mode results when the cylinder radius is shrunk to zero. These are the topologically protected one-dimensional modes in the core of the defect. Note that since we are establishing the presence of topologically protected excitations, it is sufficient to use a simple Dirac dispersion for the surface states of the strong TI since a general surface state can always be adiabatically mapped to it. We first describe the surface-Dirac Hamiltonian in the presence of curvature and apply this to the case of a cylinder with a defect inserted through it.

Dirac theory on a curved surface. On a flat surface, spanned by the unit vectors $\hat{n}_1, \hat{n}_2$, the surface-Dirac Hamiltonian for a strong TI can be taken as

$$H_{\text{flat}} = \sigma_{\tilde{1}} \hat{n}_1 \cdot \vec{p} + \sigma_{\tilde{2}} \hat{n}_2 \cdot \vec{p}, \tag{4}$$

where we assume for simplicity that the spin lies in the same plane, with a relative angle of θ to the momentum, hence $\sigma_{\tilde{1}} = (\hat{n}_1 \cos\theta + \hat{n}_2 \sin\theta) \cdot \vec{\sigma}$ and $\sigma_{\tilde{2}} = (\hat{n}_2 \cos\theta - \hat{n}_1 \sin\theta) \cdot \vec{\sigma}$. Note that for $\theta = 0$ this reduces to $H = \vec{p} \cdot \vec{\sigma}$, as in Ref. 22. In general, the σ matrices involve both spin and sublattice degrees of freedom but the essential physics is captured by taking them to be simply spin matrices.

On a curved surface there should be additional terms due to the curvature. The effective Hamiltonian can be systematically derived,[23] as described in the Appendix. Here we just present the result in the general case when the radii of curvature along the two tangent directions $\hat{n}_1, \hat{n}_2$ are R_1, R_2, respectively [which are defined via $(\hat{n}_i \cdot \vec{p})\hat{n}_j = i\hbar \delta_{ij} \hat{n}_1 \times \hat{n}_2 / R_i$ for $i = 1, 2$],

$$H_{\text{curved}} = \sigma_{\tilde{1}} \hat{n}_1 \cdot \vec{p} + \sigma_{\tilde{2}} \hat{n}_2 \cdot \vec{p} + \frac{\hbar}{2}\left(\frac{1}{R_1} + \frac{1}{R_2}\right)[\sin\theta + i \cos\theta (\hat{n}_1 \times \hat{n}_2) \cdot \vec{\sigma}]. \tag{5}$$

We now apply this result to the problem of surface states on the cylindrical surface of radius R with axis along $\hat{z}$ and radius R with strong TMI outside and vacuum inside (see Fig. 3). We use cylindrical coordinates z, ϕ, hence $\hat{n}_z = (0,0,1)$, $\hat{n}_\phi = (-\sin\phi, \cos\phi, 0)$, $\hat{n}_r = -\hat{n}_z \times \hat{n}_\phi$, and the two radii of curvature are $R_1 = \infty, R_2 = R$. For simplicity we consider $\theta = 0$. The effective Hamiltonian in the absence of a defect is

$$H_0 = (\hat{n}_z \cdot \vec{\sigma}) p_z + (\hat{n}_\varphi \cdot \vec{\sigma}) p_\varphi + \frac{\hbar}{2R} i \vec{\sigma} \cdot \hat{n}_r, \tag{6}$$

where $p_z = -i\hbar\partial_z$ and $p_\phi = -i\frac{\hbar}{R}\partial_\phi$. We can solve for the energies $H_0 \psi = E\psi$ by first performing the unitary transformation $\psi = U_z(\phi)\psi'$, where $U_z(\phi) = e^{-i\phi\sigma_z/2}$. Note that since $U_z(\phi + 2\pi) = -U_z(\phi)$, the new wave functions ψ' satisfy antiperiodic boundary conditions. The transformed Hamiltonian $H_0' = p_z\sigma_z + p_\phi\sigma_y$ has eigenvectors $\psi' = e^{ikz}e^{in\phi}\chi$, where χ is a fixed spinor. The energy eigenvalue E then satisfies

$$E_n^2(k) = \hbar^2(k^2 + n^2/R^2). \tag{7}$$

Now, due to the antiperiodicity of the ψ', we require $n + \frac{1}{2}$ to be integer. Hence, $E_n(k)$ in Eq. (7) above all correspond to massive Dirac dispersions whose mass increases as $R \to 0$.

We now consider introducing a texture in the order parameter. A strength l is readily introduced by the spin rotation $U_z(l\phi)$. The Hamiltonian then is

$$H_l = U_z^\dagger(l\phi) H_0 U_z(l\phi). \tag{8}$$

The eigenstates ψ of H_l can be obtained by the unitary transformation $\psi = U_z([l-1]\phi)\psi'$ and the transformed Hamiltonian for the wave functions ψ' is identical to H_0' above. The energy eigenvalues are then given by Eq. (7). However, the crucial difference is that the single valuedness property of the wave function now requires $n + \frac{l-1}{2}$ to be an integer. Hence, for odd values of l, when the topologically nontrivial defect is present, an $n = 0$ solution is allowed. The dispersion of this mode is $E_0(k) = \pm k$; hence there are up and down moving modes, which survive at low energies even when $R \to 0$.

The physical picture is on the surface of a cylinder the momentum p_φ is quantized according to boundary condition and the interlevel spacing is proportional to R^{-1}. Also, because of the spin-momentum relation, when electron circles about the line defect it picks up a Berry phase of $(l+1)\pi$ when the vortex winding number is l. When the total phase is an integer multiple of 2π it enforces periodic boundary condition, otherwise antiperiodic boundary condition is applied and the quantized p_φ will miss the origin. As we shrink the cylinder radius to zero, all quantized p_φ will diverge except $p_\varphi=0$. Therefore, with time-reversal symmetry a Kramers pair of line modes exists when l is odd and its dispersion only depends on p_z. Also, the distinction between the strong TMI and weak TMI can be made clear by the number of surface modes. For a weak TMI, there are even numbers of surface modes, leading to even number pairs of line modes with the above reasoning. However, they are unstable against internode scattering. In contrast, a strong TMI always has an odd number pairs of surface modes.

IV. SHANKAR MONOPOLE IN THREE DIMENSIONS

The line vortex is not the only nontrivial texture in three dimensions. The other texture we study is the Shankar monopole, a mapping $S_3 \rightarrow \mathrm{SO}(3)$ characterized by the homotopy classification $\pi_3[\mathrm{SO}(3)]=Z$.[21] Imagine an identical phase faraway from the monopole, where matrix $\overleftrightarrow{\boldsymbol{R}}(\hat{n},\varphi)$ is independent of $\hat{r}$; we can identify the infinity of real space R_3 and thus obtain S_3. As an specific example here the $\overleftrightarrow{\boldsymbol{R}}$ matrix connecting $\vec{p}$ and $\vec{\sigma}$ is $\overleftrightarrow{\boldsymbol{R}}(\hat{r},r)=\exp[i\theta(r)\hat{r}\cdot\hat{J}]$, where $\hat{r}$ and r are the directional vector and distance from the origin to the site linking i and j and $\hat{J}$ are classical rotation generators in three dimensions. The rotation axis $\hat{n}=\hat{r}$ and the rotation angle is $\theta(r)$, a function 0 at the origin and smoothly increases to $2l\pi$ $(l\in Z)$ at infinity. The homotopy class $\pi_3[\mathrm{SO}(3)]$ is described by integer l, suggesting the base manifold wraps the target manifold l times. It is protected against any continuous deformation. This is a zero-dimensional defect so the localized states should be localized charge at the monopole if any.

However, numerical results show that this topological defect does not carry localized states even in the strong TMI phase. We studied a single monopole at the center of a 32^3 unit-cell system. To treat the large system size we found a way to sidestep a complete diagonalization of the spectrum. Instead, we estimate the boundaries of the energy eigenstates using ARPACK (Arnoldi package) and shift the spectrum so that all states below (above) the band gap are at negative (positive) energies. Then, we only need to look at the difference in the number of negative- and positive-energy eigenvalues to determine the monopole charge. This can be done via an efficient LDL^T factorization, where the Hamiltonian is factorized into a lower triangular matrix L and a diagonal matrix D. The entries of the diagonal matrix preserve the sign of the eigenvalues but not their magnitude. Counting the number of positive and negative eigenvalues is then readily accomplished. While smaller system sizes sometimes show charged monopoles, at the largest sizes, they are found to be neutral. We conclude that the Shankar monopole texture does not carry charge in the TMI phase.

V. TOPOLOGICAL MOTT INSULATOR IN A MICROSCOPIC MODEL-EXTENDED HUBBARD MODEL ON THE DIAMOND LATTICE

We now discuss the question of realizing the 3D-TMI phase beginning with a microscopic model with full SRS. We consider an extended Hubbard model on the diamond lattice within mean-field theory. As always, the results of such a mean-field treatment should be treated with caution especially since strong interactions are involved. Nevertheless, we use this analytically tractable approach to obtain a range of parameters where the TMI phase is stabilized over the other obvious candidate phases—the disordered semimetal antiferromagnetic insulator [or spin-density wave (SDW)] and the charge-density wave (CDW). Realizing the 3D-TMI, which completely breaks SRS spontaneously, requires, in mean-field theory, further neighbor repulsion (between second- and third-nearest neighbors) as well as a small antiferromagnetic coupling between second neighbors, as shown in Fig. 5.

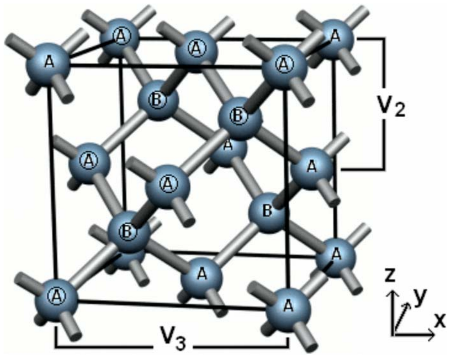

FIG. 4. (Color online) A 3D plot of diamond lattice. Each unit cell contains two sublattices, denoted by A and B, respectively, which each forms an fcc crystal. The repulsive interactions V_2 and V_3 between the second neighbor and third neighbor are shown. They are both between the atoms of the same sublattice.

We now discuss the details of this mean-field treatment. The model Hamiltonian we study is an extended Hubbard model on a 3D diamond lattice at half filling (Fig. 4),

$$H=-\sum_{\langle ij\rangle,\sigma} t(c_{i\sigma}^{\dagger}c_{j\sigma}+\mathrm{H.c.})+U\sum_{i} n_{i\uparrow}n_{i\downarrow}+\sum_{ij} V_{ij}\rho_i\rho_j + J\sum_{\langle\langle ij\rangle\rangle}\vec{S}_i\cdot\vec{S}_j,$$

where t is the nearest-neighbor hopping strength, J is the second-nearest-neighbor antiferromagnetic coupling strength between spins $\vec{S}_i=c_i^{\dagger}\vec{\sigma}c_i$, $V_{ij}=V_2$ for second-nearest-neighbor repulsion, $V_{ij}=V_3$ for third nearest-neighbor repulsion, and U is the on-site repulsion strength. All of these operate within the same sublattice as can be seen from Fig. 4. For simplicity, we assume no nearest-neighbor interaction, $V_1=0$, however, as long as V_1 (or fourth-nearest-neighbor repulsion V_4) is not so large that a nearest-neighbor charge-density wave becomes energetically favored, they can be included but will be irrelevant to our mean-field results. We neglect further neighbor interactions. $n_{i\sigma}=c_{i\sigma}^{\dagger}c_{i\sigma}$ is the number operator on site i for spin σ and $\rho_i=n_{i\uparrow}+n_{i\downarrow}-1$. Note that the Hamiltonian has full SU(2) SRS.

Without repulsive interaction the system is in a semimetal phase with gapless excitations along lines in the Brillouin zone ("Dirac lines") and a vanishing density of states at the Fermi level. We turn on interactions and investigate possible

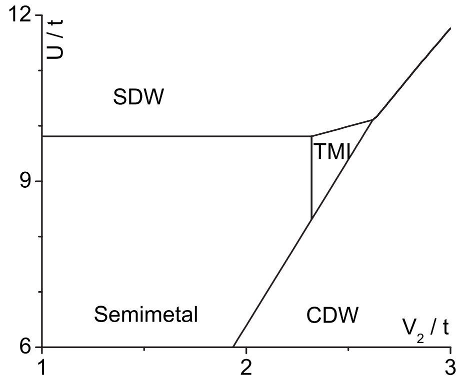

FIG. 5. Phase diagram for an extended Hubbard model on 3D diamond lattice. The phase transitions from semimetal to SDW, CDW, and TMI are all second-order transitions. Other parameters are $V_3=V_2/2$ and $J=0.3t$. The system size is $L=40$ for calculation.

phases including the TMI, second- and third nearest-neighbor CDW insulators, and nearest-neighbor SDW insulator. Note that the diamond lattice is composed of a fcc Bravais lattice plus a two-site basis that forms the two sublattices. The natural SDW phase has alternating spin densities on two sublattices, resulting from the effective antiferromagnetic coupling from nearest-neighbor hopping and U. Note that this is a $q=0$ order, i.e., preserves lattice translations. In contrast, the likely CDW orders resulting from second- and third-neighbor repulsions break translation symmetry within each sublattice. The phases can be mapped to a 3D Ising model on an fcc lattice[24] and both the second- and the third-nearest-neighbor CDWs have the same charge-density distribution for two sublattices but nonuniform distribution from unit cell to unit cell. Finally, in the TMI phase one develops second-nearest-neighbor correlations $\langle c^{\dagger}_{i\sigma}c_{j\sigma'}\rangle \sim i\vec{\sigma}_{\sigma\sigma'}\cdot\vec{\boldsymbol{R}}\cdot(\vec{d}_i\times\vec{d}_j)$ that mimic the spin-orbit interaction and break the SU(2) symmetry completely. Within the mean-field approximation we solve the ground-state energy for each phases in the following and the resulting phase diagram with fixed $J=0.3t$ is shown in Fig. 5. Note that there is a TMI phase in the center.

We now discuss the mean-field energetics of these phases in more detail.

(i) *Semimetal.* For relatively weak interactions, the semimetal phase arising from the nearest-neighbor hopping model on the diamond lattice remains stable due to the vanishing density of states at the Fermi energy. This phase retains all symmetries of the Hamiltonian.

(ii) *Spin-density wave.* In the limit of large on-site repulsion U the SDW phase with opposite spin on the two sublattices is stabilized. More precisely, if $U-24J \gg V_2$, the SDW phase becomes energetically favorable. Define the order parameter θ,

$$\langle c^{\dagger}_{i\uparrow}c_{i\uparrow}\rangle = \langle c^{\dagger}_{j\downarrow}c_{j\downarrow}\rangle = \cos^2\theta, \langle c^{\dagger}_{i\downarrow}c_{i\downarrow}\rangle = \langle c^{\dagger}_{j\uparrow}c_{j\uparrow}\rangle = \sin^2\theta.$$

The ground-state energy per unit cell is calculated using mean-field approximation

$$E_{\text{SDW}} = \frac{U}{2} + \left(\frac{U}{2} - 12J\right)\chi - \frac{1}{L^3}\sum_k \sqrt{(U-24J)^2\chi + 4|t(k)|^2}.$$

Here $\chi=\cos^2 2\theta$. $\chi=0$ denotes the semimetal phase. $t(k)=t\sum_{n=1}^{4} e^{i\vec{k}\cdot\vec{t}_n}$, $t_n=1,2,3,4$, are the vector from one atom to its nearest neighbor. L is the number of points along each direction within the first Brillouin zone.

(iii) *Charge-density wave.* In the limit of strong further neighbor repulsion V_2, V_3, a CDW is expected. The problem with just the density repulsion can be mapped to the fcc lattice Ising model. In that context it is known that V_2 will favor what is called a type-III CDW phase while V_3 will favor a type-II CDW phase,[24] as will be described below. The type-III CDW phase has Néel state in the (100) plane and frustrated arrangement between neighboring planes, which leads to a Z_2 degeneracy per plane; the type-II CDW phase can be described as a combination of four independent simple cubic CDWs. The CDW phase is important despite the frustration. As a matter of fact, in Ref. 15 the second-nearest-neighbor CDW phase, which the authors neglected, will dominate the large V_2 region and the quantum anomalous Hall phase can be realized only with inclusion of U. To suppress the CDW phases, we choose the ratio of V_3/V_2 to be 1/2 so the system is close to the transition between type-II and type-III CDW phases.[24] Hereafter we fix $V_3=V_2/2$ and point out that the phase diagram is similar without V_3 but the TMI phase will generally occur at a larger U region.

Assuming that inversion symmetry and SRS are intact, we define order parameter ρ for type-III CDW phase,

$$\langle c^{\dagger}_{1\sigma}c_{1\sigma}\rangle = \langle c^{\dagger}_{2\sigma}c_{2\sigma}\rangle = \frac{1+\rho}{2}, \quad \langle c^{\dagger}_{3\sigma}c_{3\sigma}\rangle = \langle c^{\dagger}_{4\sigma}c_{4\sigma}\rangle = \frac{1-\rho}{2},$$

where subscripts 1 and 3 are on the first sublattice of two neighboring unit cells, subscripts 2 and 4 are on the second sublattice, and σ is the spin index. The energy per original unit cell is

$$\begin{aligned} E_{\text{CDW}} &\\ &= 3V_2\rho^2 + U(1-\rho^2)/2 \\ &\quad - \frac{2}{L^3}\sum_k \sqrt{g_1^2 + |g_2|^2 + |g_3|^2 \pm \sqrt{4g_1^2|g_2|^2 + (g_2g_3^* + g_2^*g_3)^2}}, \end{aligned}$$

where $g_1=(3V_2-U/2)\rho$, $g_2=t(1+e^{i\vec{k}\cdot\vec{a}_1})$, $g_3=t(e^{i\vec{k}\cdot\vec{a}_2}+e^{i\vec{k}\cdot\vec{a}_3})$, and $\vec{a}_i$ are the lattice vectors for the fcc lattice. The momentum summation that is over $L^2/2$ points of the unit cell doubles. The CDW instability is signaled by a nonzero ρ.

(iv) *Topological Mott insulator.* More importantly, similar to the QSH phase in two dimensions,[15] at intermediate couplings the TMI phase is favored, with order parameters

$$\langle c^{\dagger}_{is}c_{js'}\rangle = i(\vec{\chi}_{ij}\cdot\vec{\sigma})_{ss'} = i|\chi|\begin{pmatrix} \cos\theta_{ij} & \sin\theta_{ij}e^{-i\varphi_{ij}} \\ \sin\theta_{ij}e^{i\varphi_{ij}} & -\cos\theta_{ij} \end{pmatrix},$$

where i,j are second-nearest neighbors. Our mean-field ansatz assumes, for simplicity, that all $\vec{\chi}_{ij}$ have the same magnitude but their directions are arbitrary and described by the angles θ_{ij} and φ_{ij}. Note $\vec{\chi}_{ij}=-\vec{\chi}_{ji}$ for hermiticity. Lattice translation, rotation, and inversion symmetries are also considered to be intact. This implies that the order parameters on the other sublattice are the negative of these. We decouple the Hamiltonian

$$H = \frac{UL^3}{2} + 24L^3(V_2 - J)|\chi|^2 - \sum_k [t(k)c_k^\dagger I_\sigma \otimes \tau^- c_k + \text{H.c.}]$$
$$- \sum_{k,\vec{d}_{ij}} 2(V_2 - J)|\chi| \sin(\vec{k}\cdot\vec{d}_{ij})[\cos\theta_{ij}(c_k^\dagger \sigma^z \otimes \tau_z c_k)$$
$$+ \sin\theta_{ij}(e^{i\phi_{ij}} c_k^\dagger \sigma^+ \otimes \tau_z c_k + \text{H.c.})],$$

where the summation is over the two occupied bands. $\vec{d}_{ij}$ are the vectors from on site to its six second-nearest neighbors (one for each opposite pair). We then obtain the ground-state energy per unit cell,

$$E_{\text{TMI}} = \frac{U}{2} + 24(V_2 - J)|\chi|^2$$
$$- \frac{2}{L^3}\sum_k \sqrt{|t(k)|^2 + 4(V_2 - J)^2|\chi|^2 \left|\sum_{\langle\langle ij\rangle\rangle} \sin(\vec{k}\cdot\vec{d}_{ij})\hat{\chi}_{ij}\right|^2},$$

where $\hat{\chi}_{ij} = (\sin\theta_{ij}\cos\phi_{ij}, \sin\theta_{ij}\sin\phi_{ij}, \cos\theta_{ij})$.

It is straightforward to see that the energy only depends on $|\chi|$ and the relative angles between $\vec{\chi}_{ij}$. Under global rotation to all $\vec{\chi}_{ij}$ the energy remains invariant and directly leads to an SU(2) degeneracy.

This is not a TMI phase in the strict sense since there are Dirac nodes at the Fermi level. However, an arbitrarily small distortion of the lattice will introduce anisotropy of nearest-neighbor hopping strengths $t_{dist}(k) = \Sigma_{n=1}^4 t_n e^{i\vec{k}\cdot\vec{\tau}_n}$ and an effective mass that leads to a gap of size δt.[6] In the simplest case that one nearest-neighbor hopping strength is different from the other three $t_{dist}(k) = t(k) + \delta t$, a stronger bond $\delta t > 0$ will lead to a strong TMI phase while a weaker bond $\delta t < 0$ will lead to a weak TMI phase.

Phase diagram. For each phase, we search for the global minimum with respect to its order parameters and compare different phases. Numerical evaluation of energies was done on a Brillouin zone with $40 \times 40 \times 40$ k space points. For simplicity we present the phase diagram with a fixed next-nearest antiferromagnetic coupling strength $J = 0.3t$ and $V_3 = 0.5V_2$ (Fig. 5). The semimetal phase exists at small U and V_2 region; the CDW phase occurs at large V_2; and the SDW phase occurs at large U. Most importantly, there is a TMI phase in the center of the phase diagram.

This TMI phase has second-nearest-neighbor correlation similar to that arising from spin-orbit interactions in the Fu-Kane-Mele model[6] on the same lattice except, of course, for an arbitrary SU(2) spin rotation, $\hat{\chi}_{ij} \sim \overleftrightarrow{\boldsymbol{R}}\cdot(\vec{d}_i \times \vec{d}_j)$, for each second-nearest-neighbor pair i and j, where $\vec{d}_i$ and $\vec{d}_j$ are nearest-neighbor bond vectors connecting this pair of sites and $\overleftrightarrow{\boldsymbol{R}}$ is an arbitrary constant three-dimensional rotation matrix.

If we further increase J the stability of the TMI phase is enhanced and it has now a wider parameter range. However, at still larger values, a different TMI phase, which breaks lattice symmetries, is realized via a continuous transition. However, since this occurs in the very large U regime, where mean-field theory may not be accurate, we do not present further details of this phase.

VI. TOWARD EXPERIMENTAL REALIZATIONS

An experimental realization of the TMI phase must contend with two challenges. First, the system should have weak intrinsic spin-orbit coupling but strong interactions. Next, the further neighbor repulsion should be substantial compared to the nearest-neighbor interactions. We believe that these difficulties can be overcome in cold-atom system, where intrinsic spin-orbit couplings are irrelevant if particles with electric multipole moments are confined to optical lattice sites. We first discuss a two-dimensional example involving electric dipoles for which a fairly definite experimental setup can be constructed. Although the phase realized here is two dimensional and does not break SRS completely [a U(1) spin rotation remains unbroken], it illustrates how the necessary ingredients can be assembled. Subsequently we discuss ideas for realizing the three-dimensional TMI, the main subject of this paper, using electric quadrupole moments.

2D case: Electric dipoles on a diamond lattice layer. Dipole-dipole interactions between heteronuclear polar molecules, such as Rb_{87} and K_{40}, have already been shown to be strong.[25] Consider a fermionic spin-1/2 molecule, with an electric dipole moment (which is independent of the spin) confined to the sites of an optical lattice. We note here that the diamond lattice has a special property that if the dipole moment is along the [100] directions then the nearest-neighbor interaction V_1 *vanishes*. Thus, the second-nearest-neighbor interaction V_2 becomes dominant. However, the difficulty is that within the 12 second-nearest neighbors, only interactions between neighbors within a plane perpendicular to the dipole moment are repulsive. This problem can be solved if we restrict the molecules within a two-dimensional (111) layer of the diamond lattice (still contain both sublattices and essentially two layers of triangular lattices) as the sites circled in Fig. 4. Then if the dipole moment is perpendicular to the plane all possible nearest-neighbor interactions are repulsive.

We solve for the mean-field phase diagram of this model, as was done previously for the 3D case. Note that since the lattice is essentially the honeycomb lattice, this is essentially the model studied in Ref. 15. There exists a 2D-TMI phase at the center of the U-V_2 phase diagram (Fig. 6). Note that this phase diagram differs from the same model in Ref. 15, which has an extended 2D-TMI phase. This is because we also allow for the second-nearest-neighbor CDW that the authors neglected. Though frustrated, this order will dominate at large V_2.

The resulting TMI phase in our case has a second-nearest-neighbor correlation resembling that of a quantum spin-Hall state and SU(2) SRS is only broken down to U(1). The resulting order parameter will be $\text{SU}(2)/\text{U}(1) = S_2$ instead of SU(2). Since $\pi_1(S_2) = 0$ there are no point topological defects, however skyrmions acquire a charge $2e$ in this phase. Note that the parameters in the phase diagram seem rather accessible for dipolar molecular systems in this setup, as-

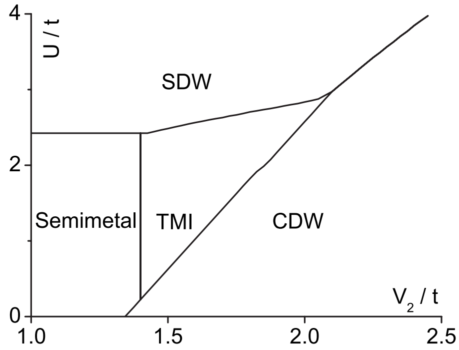

FIG. 6. Phase diagram for an extended Hubbard model on 2D diamond-lattice layer including both sublattices (essentially honeycomb lattice). Note its difference from Ref. 15. The TMI is limited to the center of the phase diagram and only partially breaks the SU(2) SRS. The system size is $L=40$ for calculation.

suming that the on-site U, which results from a combination of dipolar and microscopic interactions, is not too large.

3D-TMI: Electric quadrupoles on a distorted diamond lattice. We now discuss some ideas for realizing the 3D-TMI. While these are not as straightforward as the ones discussed earlier, we nevertheless offer them as one avenue that presents itself at the current time. Another possible origin of repulsive interaction is the quadrupole-quadrupole interaction. One can show that for two parallel uniaxial quadrupoles (quadrupole tensors are identical and diagonal), the interaction is

$$E=\frac{3Q^2}{r^5}(3-30\cos^2\theta+35\cos^4\theta),$$

where Q is the electric quadrupole moment, r is the distance between two quadrupoles, and θ is the angle between the quadrupole symmetry axis and the direction between the quadrupoles.

From this expression if $\cos^2\theta\simeq 0.742$ the quadrupole-quadrupole interaction will vanish. Therefore, assume that the quadrupole moment is along the crystal unit-cell $\hat{z}$ axis to retain as many symmetries as possible; if we elongate the lattice along one direction to make the nearest neighbors satisfy this condition, we will obtain a system where second-nearest-neighbor interaction dominates. This gives $c/a\simeq 2.40$. Note the distortion brings no change to the Hamiltonian we started with. Within this lattice, the ratio between the repulsive interaction from the second-nearest neighbor out of the quadrupole perpendicular plane and that from those in plane is $E_{\perp}/E_{\angle}=0.945$. The V_2 anisotropy is reasonably small, thus we believe that the physics we discussed with an isotropic V_2 is unchanged. However, in this arrangement, V_3 is rather small.

To give a reasonable estimate of the quadrupole strength necessary to drive the system into a TMI phase, we notice that the typical nearest-neighbor hopping strength in a cold-atom system is of order $10^{-8}\sim 10^{-6}$ K, limited by the cooling temperature, and the typical lattice dimension is about the laser wavelength 0.5×10^{-6} m. This leads to a quadrupole of $(10^{-18}\sim 10^{-17})e$ m^2, where e is unit charge. This is rather large but maybe realizable in multielectron molecules. Also, the critical quadrupole moment can be further reduced by lowering the temperature or using lasers with shorter wavelength. Finally, a moderate second-nearest-neighbor antiferromagnetic coupling may result from second-nearest-neighbor hopping superexchange effect. We leave for future work construction of a more realistic setting that can realize the 3D-TMI phase.

VII. CONCLUSION

We have argued that appropriate repulsive interactions can induce a spontaneous SRS breaking state, the TMI, where spin-orbit couplings are induced by interactions.

In addition to exotic surface states, line defects of the order parameter are found to carry protected one-dimensional modes along their length in the strong TMI, which provides a bulk signature of this phase. Also, potential experimental directions toward creating these phases in cold-atom system are discussed. An interesting open question is whether the form of the spin-orbit interactions near a line defect and hence these protected line modes can be realized by suitably modifying the atomic structure in a strong topological band insulator.

ACKNOWLEDGMENTS

We thank T. Senthil, Ari Turner, and D. H. Lee for discussions and acknowledge support from NSF under Grant No. DMR-0645691.

APPENDIX: EFFECTIVE HAMILTONIAN ON A CURVED TI SURFACE

It is known that the effective Hamiltonian for a TI surface has the form of a Dirac equation $H=\vec{p}\cdot\vec{\sigma}$ when the spin and momentum are parallel and $H=\hat{n}\cdot(\vec{p}\times\vec{\sigma})$ when they are perpendicular, where $\hat{n}$ is the normal direction of the surface. Both the momentum and spin are confined to the surface. More generally, when the angle between spin and momentum is θ the effective Hamiltonian is

$$\begin{aligned}H&=(\hat{n}_1\cdot\vec{\sigma}\cos\theta+\hat{n}_2\cdot\vec{\sigma}\sin\theta)(\hat{n}_1\cdot\vec{p})\\&\quad+(\hat{n}_2\cdot\vec{\sigma}\cos\theta-\hat{n}_1\cdot\vec{\sigma}\sin\theta)(\hat{n}_2\cdot\vec{p}),\end{aligned}$$

where $\hat{n}_1$ and $\hat{n}_2$ are orthogonal directions in plane.

One would tend to apply the same Hamiltonian to a curved surface. However, here we claim that the effective Hamiltonian on an arbitrary shaped TI surface is

$$\begin{aligned}H&=(\hat{n}_1\cdot\vec{\sigma}\cos\theta+\hat{n}_2\cdot\vec{\sigma}\sin\theta)(\hat{n}_1\cdot\vec{p})\\&\quad+(\hat{n}_2\cdot\vec{\sigma}\cos\theta-\hat{n}_1\cdot\vec{\sigma}\sin\theta)(\hat{n}_2\cdot\vec{p})\\&\quad+\frac{\hbar}{2}\left(\frac{1}{R_1}+\frac{1}{R_2}\right)\sin\theta+\frac{i\hbar}{2}(\vec{\sigma}\cdot\hat{n}_3)\left(\frac{1}{R_1}+\frac{1}{R_2}\right)\cos\theta,\end{aligned}$$

where $\hat{n}_1$ and $\hat{n}_2$ are tangent vectors of the surface with radius of curvature R_1 and R_2, respectively, and $\hat{n}_3$ is the normal vector. θ is the constant angle between spin and momentum in the corresponding flat surface effective theory. Note that when the surface is flat, the last two terms vanish and the Hamiltonian goes back to the one describing the flat surface mode.

This Hamiltonian can be systematically derived from the inclusion of the connection form for a curved space,[20,23] but an alternative method we used is to ensure hermiticity and anticommutation relation $\{H,\vec{\sigma}\cdot\hat{n}_3\}=0$ since the spin is in the surface plane,[26] with the help of the relations $(\hat{n}_i\cdot\vec{p})\hat{n}_j=i\hbar\delta_{ij}\hat{n}_3/R_i$, $(\hat{n}_i\cdot\vec{p})\hat{n}_3=-i\hbar\hat{n}_i/R_i$ for $i=1,2$ and $(\vec{\sigma}\cdot\hat{A})(\vec{\sigma}\cdot\hat{B})=\hat{A}\cdot\hat{B}+i\hat{\sigma}\cdot(\hat{A}\times\hat{B})$.

The additional terms arising from the space curvature are canceled by the inclusion of the connection form. Thus, the above effective Hamiltonian well describes a curved TI surface.

---

[1] D. J. Thouless, M. Kohmoto, M. P. Nightingale, and M. den Nijs, Phys. Rev. Lett. **49**, 405 (1982).

[2] C. L. Kane and E. J. Mele, Phys. Rev. Lett. **95**, 226801 (2005).

[3] C. L. Kane and E. J. Mele, Phys. Rev. Lett. **95**, 146802 (2005).

[4] B. Andrei Bernevig, Taylor L. Hughes, and Shou-Cheng Zhang, Science **314**, 1757 (2006).

[5] M. Konig, S. Wiedmann, C. Brne, A. Roth, H. Buhmann, L. W. Molenkamp, X.-L. Qi, and S.-C. Zhang, Science **318**, 766 (2007).

[6] Liang Fu, C. L. Kane, and E. J. Mele, Phys. Rev. Lett. **98**, 106803 (2007).

[7] J. E. Moore and L. Balents, Phys. Rev. B **75**, 121306(R) (2007).

[8] Liang Fu and C. L. Kane, Phys. Rev. B **76**, 045302 (2007).

[9] D. Hsieh, D. Qian, L. Wray, Y. Xia, Y. S. Hor, R. J. Cava, and M. Z. Hasan, Nature (London) **452**, 970 (2008).

[10] D. Hsieh, Y. Xia, L. Wray, D. Qian, A. Pal, J. H. Dil, J. Osterwalder, F. Meier, G. Bihlmayer, C. L. Kane, Y. S. Hor, R. J. Cava, and M. Z. Hasan, Science **323**, 919 (2009).

[11] A. Nishide, A. A. Taskin, Y. Takeichi, T. Okuda, A. Kakizaki, T. Hirahara, K. Nakatsuji, F. Komori, Y. Ando, and I. Matsuda, arXiv:0902.2251 (unpublished).

[12] Y. Xia, L. Wray, D. Qian, D. Hsieh, A. Pal, H. Lin, A. Bansil, D. Grauer, Y. S. Hor, R. J. Cava, and M. Z. Hasan, arXiv:0812.2078 (unpublished).

[13] H. Zhang, C.-X. Liu, X.-L. Qi, X. Dai, Z. Fang, and S.-C. Zhang, arXiv:0812.1622 (unpublished).

[14] S. Murakami, N. Nagaosa, and S. C. Zhang, Science **301**, 1348 (2003).

[15] S. Raghu, Xiao-Liang Qi, C. Honerkamp, and S. C. Zhang, Phys. Rev. Lett. **100**, 156401 (2008).

[16] T. Grover and T. Senthil, Phys. Rev. Lett. **100**, 156804 (2008).

[17] Y. Ran, Y. Zhang, and A. Vishwanath, Nat. Phys. **5**, 298 (2009).

[18] Y. Ran, A. Vishwanath, and D. H. Lee, Phys. Rev. Lett. **101**, 086801 (2008); Xiao-Liang Qi and Shou-Cheng Zhang, *ibid.* **101**, 086802 (2008).

[19] X.-L. Qi, T. L. Hughes, S. Raghu, and S.-C. Zhang, Phys. Rev. Lett. **102**, 187001 (2009).

[20] M. Nakahara, *Geometry, Topology and Physics* 2nd edition (Taylor and Francis, London, 2003).

[21] R. Shankar, J. Phys. (Paris) **38**, 1405 (1977).

[22] L. Fu and C. L. Kane, Phys. Rev. Lett. **100**, 096407 (2008).

[23] A. Sinha and R. Roychoudhury, Int. J. Theor. Phys. **33**, 1511 (1994).

[24] M. K. Phani, Joel L. Lebowitz, and M. H. Kalos, Phys. Rev. B **21**, 4027 (1980).

[25] S. Ospelkaus, K.-K. Ni, M. H. G. de Miranda, B. Neyenhuis, D. Wang, S. Kotochigova, P. S. Julienne, D. S. Jin, and J. Ye, Faraday Discuss. **142**, 1 (2009); K.-K. Ni, S. Ospelkaus, M. H. G. de Miranda, A. Pe'er, B. Neyenhuis, J. J. Zirbel, S. Kotochigova, P. S. Julienne, D. S. Jin, and J. Ye, Science **322**, 231 (2008).

[26] We thank Ari Turner for useful discussions on this point.